Available online at www.sciencedirect.com
SCIENCE DIRECT
Journal of Sound and Vibration 296 (2006) 888–907
JOURNAL OF SOUND AND VIBRATION
www.elsevier.com/locate/jsvi

Dynamics of a bowed rotor with a transverse surface crack

A.K. Darpe*, K. Gupta, A. Chawla

Department of Mechanical Engineering, Indian Institute of Technology, Delhi 110016, India

Received 15 December 2004; received in revised form 19 February 2006; accepted 16 March 2006
Available online 23 May 2006

Abstract

The rotors in industrial installations have various faults that could simultaneously exist and sometimes cannot be removed altogether, although efforts are always made to keep them within the acceptable limits (e.g., unbalance, misalignment, etc). Researchers in the past have mostly modelled and analysed individual fault separately and assumed a simplified rotor model and support conditions. In this paper, the equations of motion of the rotor with a transverse surface crack with a bow are formulated and steady state and transient response analysis of the rotor is attempted. The purpose of the study is to assess the effect of the residual bow on the stiffness characteristic of the rotating cracked shaft and changes if any, qualitative and/or quantitative that a bow may bring about in the dynamics of a cracked rotor. It has been observed that the usual level of bow may not significantly influence the stiffness variation and the nonlinear nature of crack response is not significantly altered. However, the bow completely masks the sensitivity of orbital response of cracked rotor to unbalance phase at half the critical speed and the use of influence of unbalance phase on orbital response at half critical speed of cracked rotor cannot be used for the detection purposes. The directional nature of higher harmonics such as $3\times$ frequency component and their amplitude do not significantly alter. Due to the presence of crack and under the influence of gravity, the zero response at the self-balancing speed of the bowed rotor for a specific phase of unbalance is not observed.

1. Introduction

The effect of the presence of the single transverse crack on the response of the rotor has been a focus of attention for many researchers. If undetected early, such cracks can pose a potential source of catastrophic failures. Several researchers have therefore conducted extensive investigations on the response of cracked rotor over the last three decades. An in depth literature review of dynamics of cracked rotors was published by Wauer [1] and later a more exhaustive state of the art review on rotors as well as structures was published by Dimarogonas [2]. Gasch [3] provided a survey of the stability behaviour and forced vibrations of a rotating shaft with crack. Gupta [4] reviewed various diagnostic strategies for transverse crack in rotor shaft and blades and discussed their limitations and advantages in order to evolve effective crack detection techniques. He also outlined improvements to enhance applicability of these strategies to real systems. Recently, Sabnavis et al. [5] have reviewed the literature on cracked shaft detection and diagnosis that appeared after 1990. While several

*Corresponding author.
E-mail address: akdarpe@mech.iitd.ernet.in (A.K. Darpe).

0022-460X/$ - see front matter © 2006 Elsevier Ltd. All rights reserved.
doi:10.1016/j.jsv.2006.03.013

authors [3,6,7] mainly focussed their work on unbalance lateral vibration response of the cracked rotor, others [8–10] investigated and proposed new methods of crack detection based on coupling of vibration due to the presence of crack in a rotor.

There are several hundred research papers addressing dynamics of cracked rotors and identification of crack. However, a rotor is typically having several faults like unbalance, misalignment, bearing nonlinearity etc. Thus a rotor bearing system is essentially a multi-fault system and it is important to isolate individual faults from the vibration signal. Apart from including unbalance as another fault, most of the studies do not account for the presence of any other fault while investigating the crack modelling and its response.

Broad review of the state of the art in fault diagnosis techniques, with particular regard to rotating machinery has been presented by Edwards et al. [11]. The unbalance, bowed shafts and cracked shafts are the more common rotor dynamic faults [11]. Platz and Markert [12] have presented some fault models for detecting important rotor faults such as crack, unbalance, rub, bow, misalignment and rotor asymmetry. These fault models form the basis for the model-based fault identification.

In this paper a systematic modelling of more than two faults is attempted and the response of a cracked rotor with bow is analysed in the presence of unbalance. A rotor bow can be caused by different factors and the bow can cause severe rubbing between stator and rotor. In many rotor applications, a residual bow in the shaft may be induced due to various reasons, namely, gravity sag, thermal distortions, shrink fits, mechanical bow due to prior unbalance, etc. Some of these are temporary and some are permanent in nature. Shrink fits and thermal bow due to prolonged rubbing of shafts on seals normally lead to a long lasting residual bow. During start up of hot turbomachinery, such as gas turbines, steam turbines and water pumps in nuclear reactors, a bow can be developed in the rotor shaft due to an asymmetric heat distribution. This may be caused by partial steam inlet conditions in a steam turbine. The gravitational sag of the rotor may produce a temporary mechanical bow in the shaft.

A systematic study on the effect of bow has been carried out by Nicholas et al. [13] wherein the effect of phase of bow has been investigated on the phase and response of the rotor. Based on transfer matrix method, Salamone [14] investigated the unbalance response of a rotor with a skewed disk, in addition to shaft bow. Flack and Rooke [15] compared the theoretical and experimental synchronous unbalance response of a Jeffcott rotor with bow on different types of fluid film bearings using transfer matrix method. Flack et al. [16] investigated the rotor response with run-out, bow and unbalance, both theoretically and experimentally. Gnielka [17] discussed modal balancing procedure for multibearing rotor system with initial bow and verified it through experimentation. Parkinson et al. [18] also investigated response of rotating shaft with mass unbalance and bow and proposed what he called the net whirl (total whirl minus shaft bow) balancing. The complex modal balancing of shafts with an initial bow has been developed by Meacham et al. [19]. Nelson [20] presented a balancing procedure for a multi-degree-of-freedom system including the effects of residual bow. The method however, required the knowledge of the mathematical model of the system. Rao [21] investigated response of the bowed rotor and made several observations regarding detection of the bow, emphasising the use of phase information. Ehrich [22] discussed the effect of bow on the dynamics of the rotor. Goldman and Muszynska [23] and Goldman et al. [24] modelled the thermal/mechanical effects of the rotor-stator rub and the related introduction of rotor bow due to localised heating effect. Edwards et al. [25] used excitation due to bent rotor and unbalance in the model to identify support parameters of the rotor bearing foundation system and could identify the bend in the rotor.

More often than not, the main assumptions involved in the modelling and analysis are the simplicity of rotor bearing system. The cracked rotor is assumed simply supported and the damping, flexibility or any other nonlinear effects at the support are not accounted for in the mathematical model of the rotor system. Another important aspect of modelling is that, apart from the unbalance no other fault is assumed in the system. However, the rotors in industrial installations have various other faults that cannot be removed altogether, although efforts are always made to keep them within the acceptable limits. There can be tolerable levels of misalignment of the coupled rotors, temporary bow due to variety of reasons, bearing nonlinearity, asymmetric stiffness of rotor parts or supports, to name a few. A lot of efforts go into tackling these aspects at the design stage. However during the coarse of time, one or more of these faults creep into the system. Sometimes prolonged existence of one fault may lead to the development of another fault. For example, severe misalignment preloads may cause cracking or an unnoticed persistent rotor rubbing may induce thermal bow

in the rotor. In such situations, when more than one fault may exist in the rotor bearing system, the problem of relating the observed vibration response to a particular fault could become a rather difficult task. In the recent past only a few of research studies have addressed this problem.

Bachschmid and Pennacchi [26], Platz et al. [27], and Bachschmid et al. [28] worked on model-based diagnosis of more than one fault existing in the rotor system. They presented fault models for rotor bow and coupling misalignment, etc. and investigated identification of a fault when unbalance and moments (simulating several types of faults) act in the rotor system. They used least square fitting approach by means of minimisation of multidimensional residual between the vibrations in some measuring planes. They have shown that the method effectively estimates the location and severity of one or two simultaneous faults. For one fault, identification is almost perfect, but, for two faults [28] the error as low as 2% and as high as 66% are reported for some of the cases. Pennacchi and Vania [29] analysed the transient vibrations of a generator rotor that was affected by a thermal bow and through the model-based fault identification procedure, could separate the bow from the unbalance symptoms rather accurately. On the other hand, Darpe et al. [30] addressed signal based identification of faults for multi-fault rotor. They developed a two-crack Jeffcott rotor model wherein multiple faults such as unbalance, crack and rotor stiffness asymmetry were modelled. Through orbital and frequency domain plots they proposed different diagnostic features to separate rotor asymmetry from rotor crack although the two faults are typically known to produce similar vibration signals. Wan et al. [31] have investigated vibration of a cracked rotor-sliding bearing system with rotor stator rub, using harmonic wavelet transform (HWT). They observed differences in wavelet time–frequency maps of cracked rotor with and without rubbing. Although, they have not separated out the distinguishing features related to crack and rubbing, this is one of the few studies where two faults have been accounted in the rotor model apart from unbalance.

In the present study, the equations of motion of the rotor with a transverse surface crack with a bow are formulated. Preliminary analysis involving the phase of bow relative to the crack direction is attempted. The purpose of the study is to assess the effect of the residual bow on the stiffness characteristic of the rotating cracked shaft and changes if any, qualitative and/or quantitative that a bow may bring about in the dynamics of cracked rotor. There have been several instances (e.g., Ref. [32]) when the cracked rotors were reported to have a slight bow. Thus, it is important to understand in what way the induced bow influences the vibration response of the cracked rotor and how the bow would affect the breathing (closing and opening) behaviour of the cracked rotor. Since crack breathing is the prime source of nonlinearity associated with crack in a rotor, this issue needs to be investigated.

2. Equations of motion for the cracked rotor with bow

Consider a Jeffcott rotor rotating at a constant speed ω, mounted on rigid bearing support and having a disc of mass m at the centre of the span of length L. Let the shaft diameter be D meters and centre of mass assumed away from the geometric centre at a distance ε. The shaft has a transverse surface crack of depth a near midspan. The strong crack direction is represented by η and the weak crack direction by ξ. These are also the rotor fixed coordinates (Fig. 1). Let the unbalance orientation angle relative to crack direction be β. The shaft has a residual permanent bow of magnitude R_o at an angle ψ from the ξ-axis as shown in the figure. The equations of motion can be written as follows.

$$\begin{aligned} &m\ddot{\xi} + c\left(\dot{\xi} - \omega\eta\right) - 2\omega\dot{\eta}m - m\omega^2\xi + k_{\xi}(\xi - R_0\ \cos\ \psi) + k_{\xi\eta}(\eta - R_0\ \sin\ \psi) = m\varepsilon\omega^2\cos\beta - mg\ \cos\ \omega t,\\ &m\ddot{\eta} + c(\dot{\eta} + \omega\xi) + 2\omega\dot{\xi}m - m\omega^2\eta + k_{\eta\xi}(\xi - R_0\ \cos\ \psi) + k_{\eta}(\eta - R_0\ \sin\ \psi) = m\varepsilon\omega^2\sin\beta + mg\ \sin\ \omega t. \end{aligned} \quad (1)$$

The solution scheme to solve the above equations is detailed in Ref. [33]. However, it is briefed here for the sake of completeness. As the cracked rotor rotates, the crack breathes. The amount of open part of the crack constantly changes, thereby changing the stiffness of the cracked rotor. Obviously the stiffness at any instant is proportional to the amount of open part of the crack. Stiffnesses in Eq. (1) are response dependent, as the breathing model considered here estimates the stiffness at each instant of time from the response of the rotor at the previous instant. This causes the above equations to be non-linear, as the response (ξ, η) is used to find new stiffness values (k_{ξ}, k_{η}, $k_{\xi\eta}$ and $k_{\eta\xi}$) that are used in Eq. (1) to find the next set of response (ξ, η). Since the

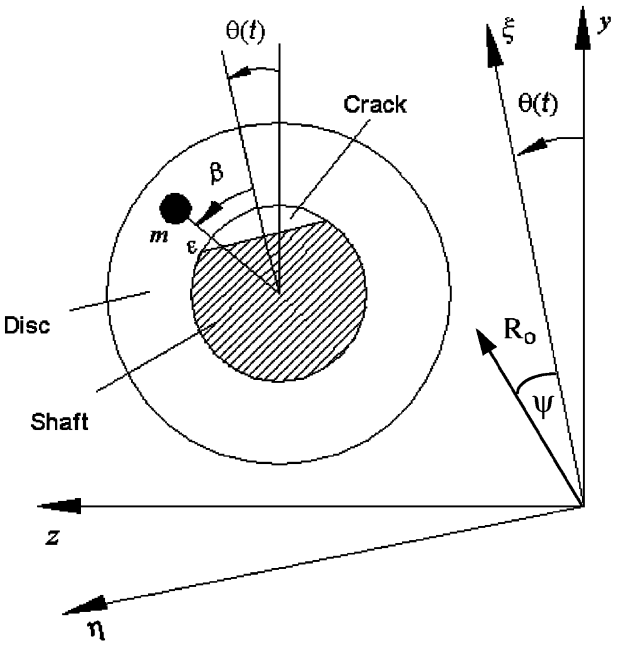

Fig. 1. Coordinate system showing the bow vector.

partial crack opening is considered in this model, it is necessary to devise a strategy to estimate the open and closed part of the crack at any instant. This is found using the stress field along the crack tip. The stress intensity factor (SIF), which is indicative of the magnitude of this stress field, varies along the crack edge and is a function of both forces (Q_ξ and Q_η) acting on the rotor at the crack location (Fig. 2) and the position along the crack edge, w (Fig. 3). The sign of SIF gives indication of the open or closed state of the crack. Negative SIF indicates compressive stress field and the crack is closed at that point along the crack tip, whereas a positive SIF indicates tensile stress field and the crack in an open state. The SIF is estimated with the assumption of pure bending and no shear deformation.

The total stress intensity factor K^I is expressed as follows [7], [34]:

$$K^I = K^I_{Q_\xi} + K^I_{Q_\eta}. \tag{2}$$

Here,

$$K^I_{Q_\xi} = \sigma_\xi \sqrt{\pi\alpha} F(\alpha/\alpha'), \quad K^I_{Q_\eta} = \sigma_\eta \sqrt{\pi\alpha} F'(\alpha/\alpha') \tag{3}$$

are the SIF due to Q_ξ and Q_η, respectively. Here σ_ξ and σ_η are the bending stresses due to Q_ξ and Q_η, respectively. These are given by

$$\sigma_\xi(w) = \frac{(Q_\xi L/4)(\alpha'/2)}{I}, \quad \sigma_\eta(w) = \frac{(Q_\eta L/4)w}{I}, \tag{4}$$

where $I = ((\pi/64)D^4)$ and $\alpha' = \sqrt{D^2 - (2w)^2}$, and the functions F and F' are given by

$$F(\alpha/\alpha') = \sqrt{\frac{2\alpha'}{\pi\alpha}\tan\left(\frac{\pi\alpha}{2\alpha'}\right)}\,\frac{0.923 + 0.199[1 - \sin(\pi\alpha/2\alpha')]^4}{\cos(\pi\alpha/2\alpha')}, \tag{5}$$

$$F'(\alpha/\alpha') = \sqrt{\frac{2\alpha'}{\pi\alpha}\tan\left(\frac{\pi\alpha}{2\alpha'}\right)}\,\frac{0.752 + 2.02(\alpha/\alpha') + 0.37[1 - \sin(\pi\alpha/2\alpha')]^3}{\cos(\pi\alpha/2\alpha')}. \tag{6}$$

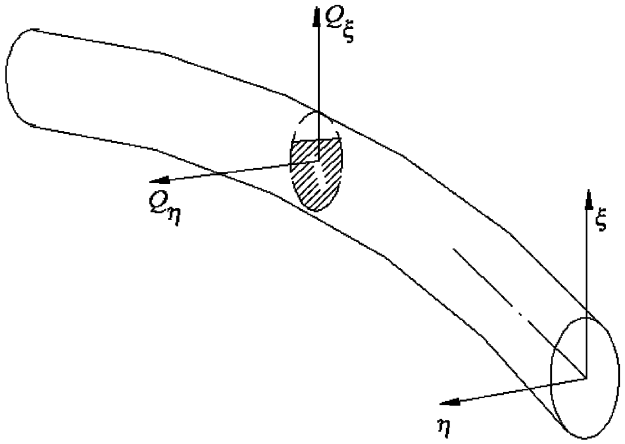

Fig. 2. Forces acting on the rotor at the location of the crack.

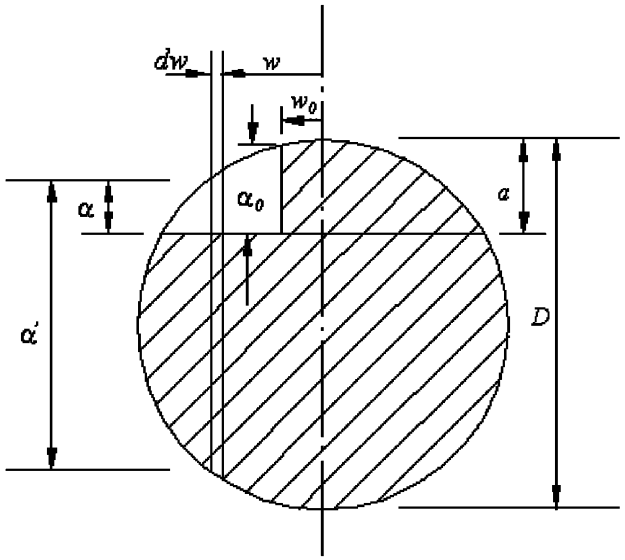

Fig. 3. Details of the cross section of the rotor at the location of crack.

After finding the sign of SIF at various locations along the crack edge using Eq. (2), the position where the SIF changes its sign can be found. This position separates the open and closed areas of crack face. The next step is to find the stiffness of the cracked rotor using this information. First, an additional displacement corresponding to additional strain energy due to the presence of crack is expressed. Thus the flexibility of the shaft due to crack can be found. When added with the flexibility of the uncracked shaft, it gives the total flexibility of the cracked shaft. The stiffness of the cracked rotor in the two lateral directions can then be found.

For a prismatic bar of unit width and height α' with a crack of depth a, under general loading, the additional displacement u_i along the direction of force Q_i due to the presence of crack can be computed using Castingliano's theorem. Thus if U^c is the additional strain energy due to a crack,

$$u_i = \frac{\partial U^c}{\partial Q_i}. \tag{7}$$

The strain energy due to crack can be written as

$$U^c = \int_0^a J(a)\,\mathrm{d}a, \tag{8}$$

where $J(a) = \left(\partial U^c/\partial a\right)\,\mathrm{d}a$ is a strain energy density function. Thus, substituting $J(a)$ in Eqs. (7) and (8), we get

$$u_i = \frac{\partial}{\partial Q_i}\int_0^a J(a)\,\mathrm{d}a. \tag{9}$$

The strain energy density function has the general form,

$$J = \frac{1}{E'}\left[\left(\sum_{i=1}^{6} K_i^{\mathrm{I}}\right)^2 + \left(\sum_{i=1}^{6} K_i^{\mathrm{II}}\right)^2 + m_s\left(\sum_{i=1}^{6} K_i^{\mathrm{III}}\right)^2\right], \tag{10}$$

where K^i, $i = \mathrm{I}, \mathrm{II}, \mathrm{III}$, are SIFs.

$m_s = (1+\upsilon)$, υ is Poisson's ratio and $E' = E/(1-\upsilon^2)$, E is Young's modulus.

Considering only pure bending of the shaft in the two lateral directions without any shear stresses and considering only opening mode (mode I) crack displacements (neglecting crack displacements in other modes such as shearing (mode II) and tearing (mode III)), Eq. (10) gets modified to

$$J(\alpha) = \frac{1}{E}\left(K_{Q_\xi}^I + K_{Q_\eta}^I\right)^2. \tag{11}$$

Thus, the additional displacement due to crack for a prismatic beam can be written as

$$u_i = \frac{1}{E}\frac{\partial}{\partial Q_i}\int_0^a \left(K_{Q_\xi}^I + K_{Q_\eta}^I\right)^2 \mathrm{d}a. \tag{12}$$

When a solid shaft with a transverse crack is assumed to comprise of several such thin prismatic beams with depth α' and crack depth α that change along the width w, the additional displacement of the cracked shaft is given by integrating along the width of the crack.

The additional displacement in direction ξ can be written as follows:

$$u_\xi = \frac{1}{E}\frac{\partial}{\partial Q_\xi}\int_{-b}^{b}\int_0^\alpha \left(K_{Q_\xi}^I + K_{Q_\eta}^I\right)^2 \mathrm{d}\alpha\,\mathrm{d}w. \tag{13}$$

Thus the additional flexibility g_ξ in the direction ξ due to the force Q_ξ can be written as $g_\xi^c = \partial u_\xi/\partial Q_\xi$, which using Eqs. (13) and (3) can be written as

$$g_\xi^c = \int\!\!\int \frac{128L^2\alpha'^2\alpha}{E\pi D^8} F\left(\alpha/\alpha'\right)^2 \mathrm{d}\alpha\,\mathrm{d}w. \tag{14}$$

Other crack flexibility values can be easily found as given below

$$g_\eta^c = \int\!\!\int \frac{512L^2w^2\alpha}{E\pi D^8} F'\left(\alpha/\alpha'\right)^2 \mathrm{d}\alpha\,\mathrm{d}w. \tag{15}$$

$$g_{\xi\eta}^c = \int\!\!\int \frac{256L^2\alpha' w}{E\pi D^8}\alpha F\left(\alpha/\alpha'\right)F'\left(\alpha/\alpha'\right)\mathrm{d}\alpha\,\mathrm{d}w. \tag{16}$$

Now adding flexibility of uncracked shaft to the additional flexibility due to the crack as discussed above, we obtain following flexibility coefficients:

$$g_\xi = \frac{L^3}{48EI} + \iint \frac{128L^2\alpha'^2\alpha}{E\pi D^8} F\left(\alpha/\alpha'\right)^2 \,\mathrm{d}\alpha\,\mathrm{d}w,$$
$$g_\eta = \frac{L^3}{48EI} + \iint \frac{512L^2w^2\alpha}{E\pi D^8} F'\left(\alpha/\alpha'\right)^2 \,\mathrm{d}\alpha\,\mathrm{d}w,$$
$$g_{\xi\eta} = g_{\eta\xi} = \iint \frac{256L^2\alpha' w}{E\pi D^8} \alpha F\left(\alpha/\alpha'\right) F'\left(\alpha/\alpha'\right) \,\mathrm{d}\alpha\,\mathrm{d}w. \tag{17}$$

Using the above flexibility values, following stiffness values are obtained:

$$k_\xi = \frac{g_\eta}{g_\xi g_\eta - g_{\xi\eta}^2}, \quad k_\eta = \frac{g_\xi}{g_\xi g_\eta - g_{\xi\eta}^2}, \quad k_{\xi\eta} = k_{\eta\xi} = \frac{-g_{\xi\eta}}{g_\xi g_\eta - g_{\xi\eta}^2}. \tag{18}$$

It may be noted that these stiffness values are found after the integration limits in the flexibility expressions are decided upon finding the open part of the crack. The open part of the crack is estimated based on the sign of SIF along the crack edge. It may be recalled from Eqs. (3) and (4) that the SIF is a function of forces on the rotor. These forces can be related to the response of the rotor using following equation:

$$Q_\xi = k_\xi\xi + k_{\xi\eta}\eta, \quad Q_\eta = k_{\eta\xi}\xi + k_\eta\eta. \tag{19}$$

Thus the stiffness values are estimated using the response of the rotor and these new stiffness values are used back again in the equation of motion to obtain new set of rotor response to be again used to estimate new stiffness values. Thus the equations of motion in this case are response dependent, nonlinear.

Substituting $2m\varsigma\omega_0$ for c in the Eq. (1),

$$\ddot{\xi} + 2\varsigma\omega_0\left(\dot{\xi} - \omega\eta\right) - 2\omega\dot{\eta} - \left(\omega^2 - \omega_\xi^2\right)\xi + \omega_{\xi\eta}^2\eta = \varepsilon\omega^2 \cos\beta - g\cos\omega t + R_0\omega_\xi^2\cos\psi + R_0\omega_{\xi\eta}^2\sin\psi,$$
$$\ddot{\eta} + 2\varsigma\omega_0(\dot{\eta} + \omega\xi) + 2\omega\dot{\xi} - \left(\omega^2 - \omega_\eta^2\right)\eta + \omega_{\xi\eta}^2\xi = \varepsilon\omega^2 \sin\beta + g\sin\omega t + R_0\omega_\eta^2\sin\psi + R_0\omega_{\xi\eta}^2\cos\psi. \tag{20}$$

Here ς is damping factor and

$$\delta_{st} = mg/k_0, \quad \omega_\xi = \sqrt{\frac{k_\xi}{m}}, \quad \omega_\eta = \sqrt{\frac{k_\eta}{m}},$$
$$\omega_{\xi\eta} = \sqrt{\frac{k_{\xi\eta}}{m}}, \quad \omega_{\eta\xi} = \sqrt{\frac{k_{\eta\xi}}{m}}, \quad \omega_0 = \sqrt{\frac{k_0}{m}} \tag{21}$$

where k_0 is the stiffness of uncracked rotor.

Introducing the following dimensionless parameters,

$$\bar{\xi} = \xi/\delta_{\mathrm{st}},\ \bar{\eta} = \eta/\eth_{\mathrm{st}},\ \bar{R}_o = R_o/\delta_{\mathrm{st}},\ \tau = \omega t,\ e = \varepsilon/\delta_{\mathrm{st}},$$
$$r_0 = \omega_0/\omega,\ r_\xi = \omega_\xi/\omega,\ r_\eta = \omega_\eta/\omega,\ r_{\xi\eta} = \omega_{\xi\eta}/\omega,\ r_{\eta\xi} = \omega_{\eta\xi}/\omega \tag{22}$$

Eq. (20) can be non-dimensionalised as

$$\ddot{\bar{\xi}} + 2\zeta r_0(\dot{\bar{\xi}} - \bar{\eta}) - 2\dot{\bar{\eta}} - \left(1 - r_\xi^2\right)\bar{\xi} + r_{\xi\eta}^2\bar{\eta} = e\cos\beta - r_0^2\cos\tau + \bar{R}_o r_\xi^2\cos\psi + \bar{R}_o r_{\xi\eta}^2\sin\psi,$$
$$\ddot{\bar{\eta}} + 2\zeta r_0(\dot{\bar{\eta}} + \bar{\xi}) + 2\dot{\bar{\xi}} + \left(r_\eta^2 - 1\right)\bar{\eta} + \bar{\xi}r_{\eta\xi}^2 = e\sin\beta + r_0^2\sin\tau + \bar{R}_o r_\eta^2\sin\psi + \bar{R}_o r_{\eta\xi}^2\cos\psi. \tag{23}$$

Thus the equations have bow forces apart from the gravity and unbalance forces on the right-hand side. The solution of these equations is iterative since the forces of unbalance, gravity and bow together influence the crack status. The time step in 4th order Runge Kutta method of numerical integration is 0.00001301 s. The stiffness values are assumed constant for time equal to one degree of rotation.

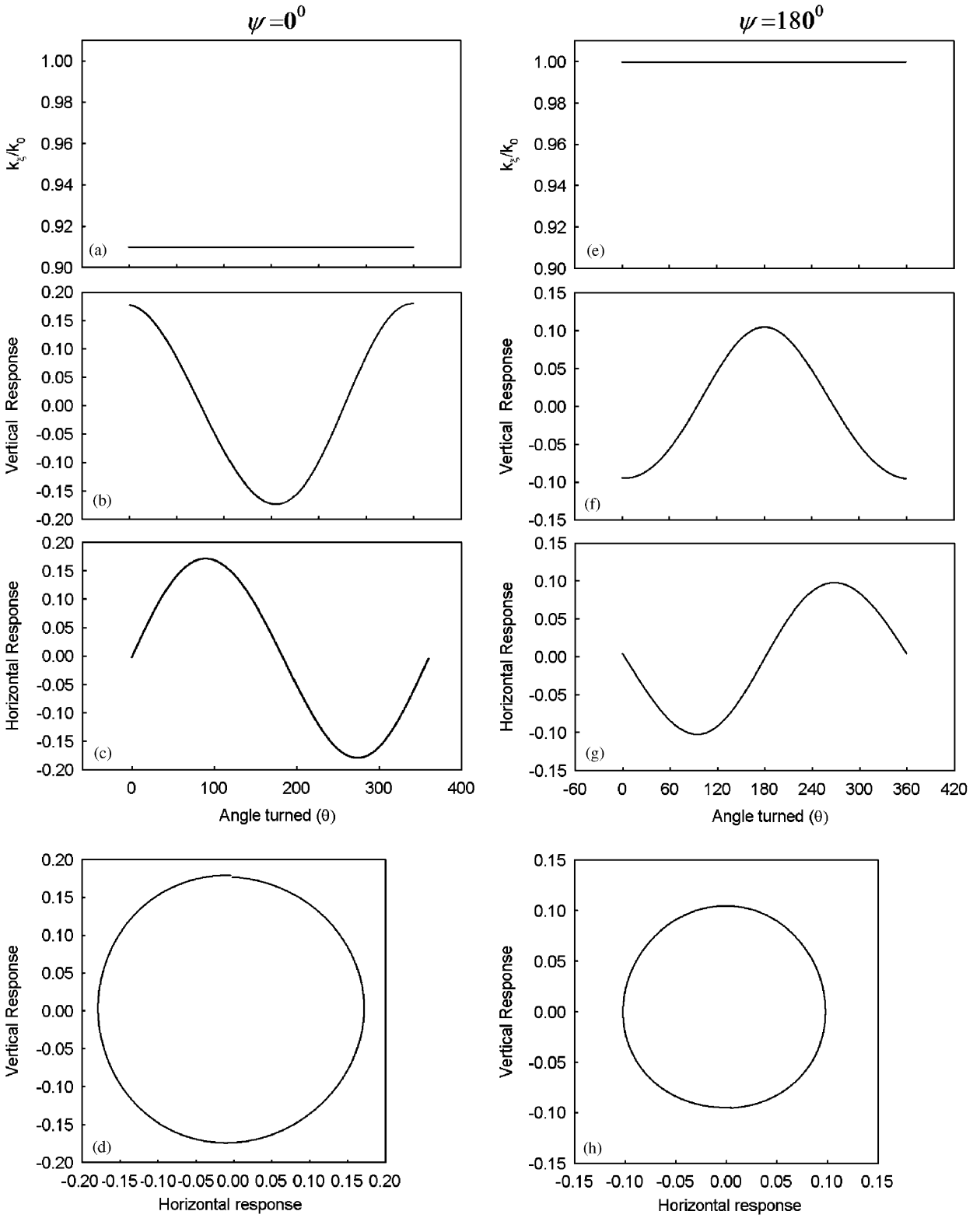

Fig. 4. Stiffness ratio variation, time domain response and orbit plot of the cracked bowed rotor neglecting gravity, with $\psi = 0^\circ$ and 180°.

3. Unbalance response of the cracked bowed rotor

A simply supported cracked Jeffcott rotor with length $L = 0.7\,\text{m}$, diameter $D = 0.015\,\text{m}$ and a central disc of mass $m = 1\,\text{kg}$ is considered. The crack depth ratio of $\bar{a} = 0.4$ and bow intensity of $\bar{R}_0 = 1.0$ is assumed. Fig. 4 shows the response of cracked bowed rotor at $r_{\text{unb}} = 0.5$ for two different cases of bow phase ($\psi = 0^\circ$ and $\psi = 180^\circ$). The phase of unbalance relative to the crack (β) is assumed to be 0° in all the simulations unless otherwise stated. The effect of gravity is neglected in this particular case. For $\psi = 0^\circ$, the stiffness ratio (k_ξ/k_0) variation is a straight line and the ratio is of constant value of 0.91 (Fig. 4a). The bow is in phase with the crack and hence tends to keep the crack open. The cracked rotor despite rotating at 1/2 the critical speed does not show second harmonic component in the lateral vibration response, which looks almost like pure sinusoidal waveform (Figs. 4b and c). It may be noted that the $2\times$ frequency component in the case of cracked rotor is due to gravity and hence is absent in this case as gravity is neglected in the analysis. The orbit plot is a circle, as expected (Fig. 4d).

When the bow phase is opposite the crack direction ξ ($\psi = 180^\circ$), the bow tends to close the crack and hence the stiffness ratio variation is a straight line with $k_\xi/k_0 = 1.0$ (Fig. 4e). It may be recalled that the stiffness ratio $k_\xi/k_0 = 1$ indicates a fully closed crack. The lateral vibration response in this case is no different than for $\psi = 0^\circ$, however, there is a marked reduction in the peak to peak amplitude of the response in vertical and horizontal directions as the bow tends to limit the response (Figs. 4f and g). The phase of the response is completely different from the previous case as evident from the time domain response (Figs. 4b,c,f and g). The orbit plot is reduced in size (Fig. 4h).

When the gravity is accounted in the analysis, there are considerable changes in the response of the rotor system (Fig. 5). The cracked rotor response at 1/2 the critical speed shows very prominent presence of $2\times$ frequency component and looped orbit, which is well known. Fig. 5 shows marked changes in the vertical and horizontal lateral vibration response (Figs. 5b and c) showing $2\times$ frequency component compared to predominantly $1\times$ frequency response in the earlier no-gravity case (Figs. 4b and c). The stiffness variation is also showing characteristic crack breathing with gradual decrease and increase of stiffness ratio (Fig. 5a). The orbit plot shows a double looped orbit (Fig. 5d). When the phase of bow is opposite the crack, the $2\times$ frequency component dominates the response and the looped orbit (Fig. 5h) becomes quite similar to the orbit of an asymmetric rotor. In this case of bow vector opposite to the crack direction, the bow tends to limit the deflection of the rotor due to additional flexibility induced due to presence of crack. This effectively reduces the $1\times$ component of the rotor response and accentuates the $2\times$ response due to stiffness asymmetry induced due to crack. Darpe et al. [30] have shown that if a transverse crack develops in an asymmetric rotor, it shows up in the form of changed orbit plot of the rotor. The close loops in the asymmetric rotor changes to a smaller inner loop due to added flexibility of the crack. However, the above results show that the presence of crack may not produce any changes in the orbit of the asymmetric rotor if a bow exists out of phase of the crack.

When the bow phase ψ is at 90° or 270° to the crack direction, the change in the response is not apparent from the time domain response (Figs. 6b,c,f and g). However, the orbit plot shifts orientation and the inner loop gets oriented in the direction of bow (Figs. 6d and h). The size of the inner loop is larger compared to the one for $\psi = 0^\circ$ and smaller compared to the one for $\psi = 180^\circ$.

When the bow is very large $\left(\bar{R}_0 = 10\right)$, the influence of the bow on the stiffness variation is quite significant (Fig. 7). Thus when the bow is in phase with the crack the crack tends to remain always open despite the presence of gravity force. The $2\times$ frequency component is present but is quite small compared to the $1\times$ component (Figs. 7c,d). The looped orbit is not observed (Fig. 7e). When the bow is out of phase with the crack, the crack tends to remain always closed. Obviously the $2\times$ frequency component is almost absent in the frequency spectra (Fig. 7h,i). However, it may be noted that such large bow amplitude is not expected in practice and the gravity will always dominate the response of the cracked bowed rotor.

The influence of the unbalance phase (β) on the response of the cracked bowed rotor is investigated. Fig. 8 shows the orbit plot for various values of β for a constant value of bow phase ($\psi = 0^\circ$). The figure indicates negligible influence of the unbalance phase on the orbit plot of the cracked bowed rotor with the orbit plot with inner loop oriented more or less in the same orientation. Fig. 8 also shows the influence of the unbalance phase on the cracked rotor without bow. In absence of bow, the unbalance phase influences the response of cracked rotor at second harmonic resonant speed. This influence is observed in the form of variation in inner

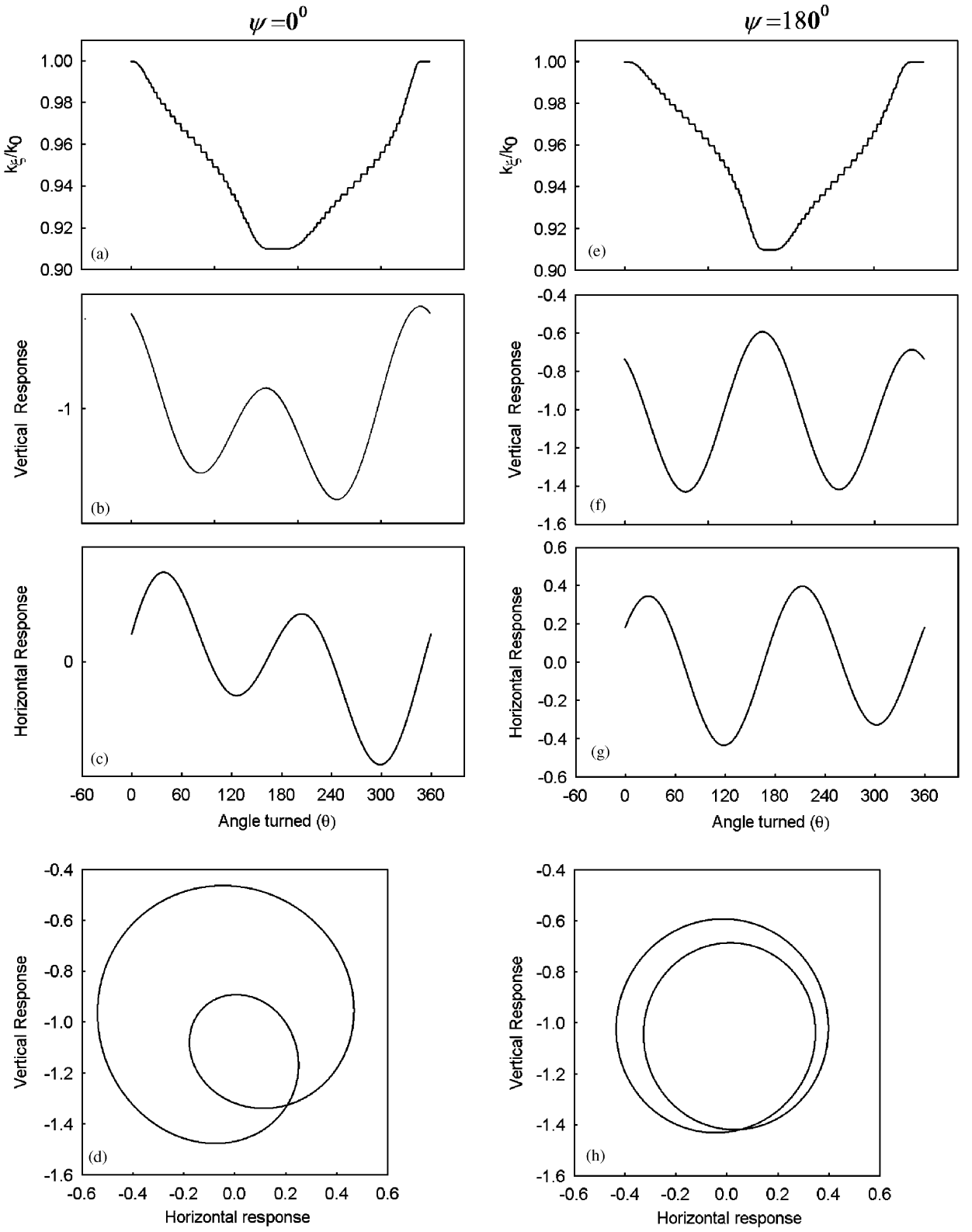

Fig. 5. Stiffness ratio variation, time domain response and orbit plot of the cracked bowed rotor considering gravity, with $\psi = 0^\circ$ and 180°.

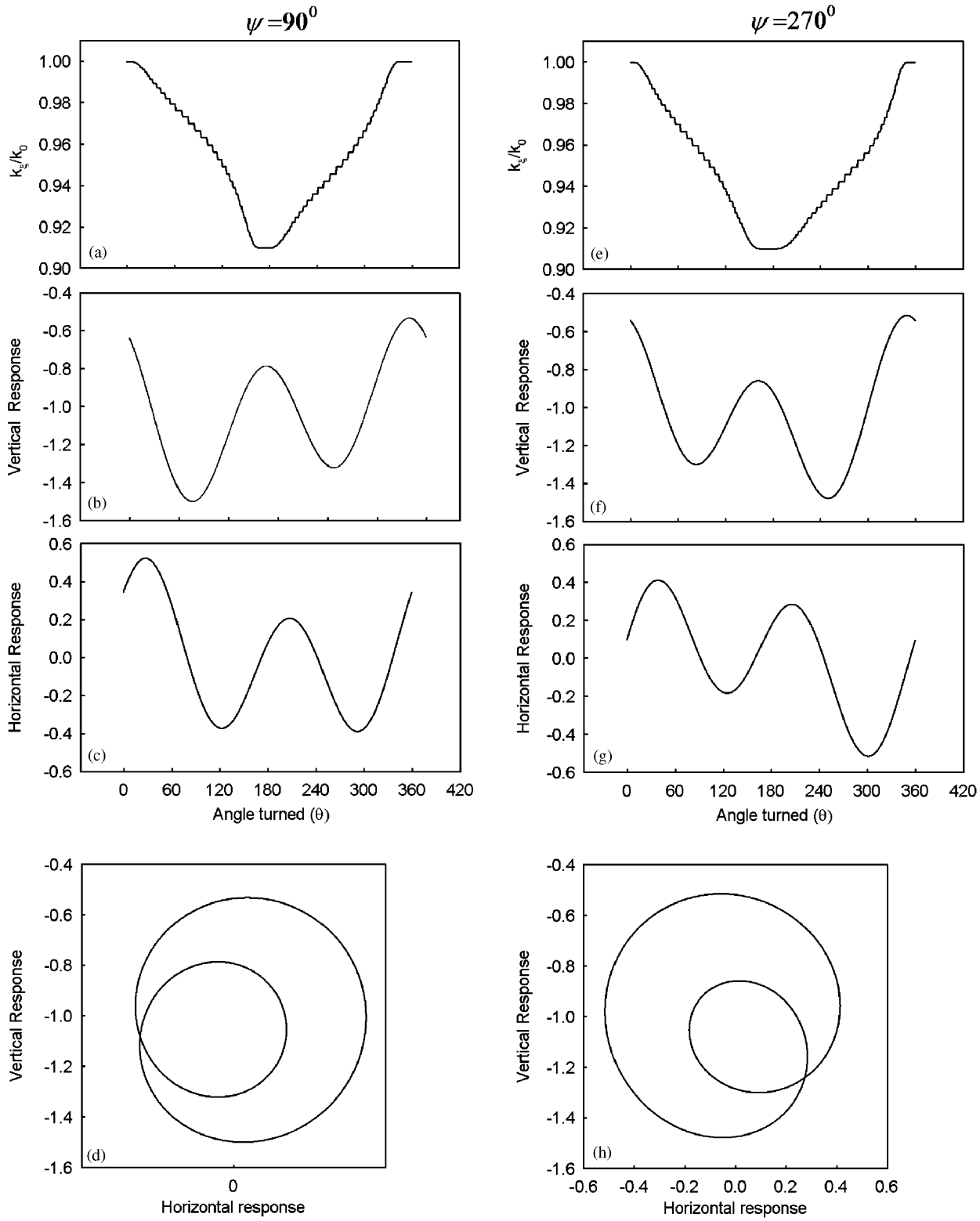

Fig. 6. Stiffness ratio variation, time domain response and orbit plot of the cracked bowed rotor considering gravity, with $\psi = 90^\circ$ and 270°.

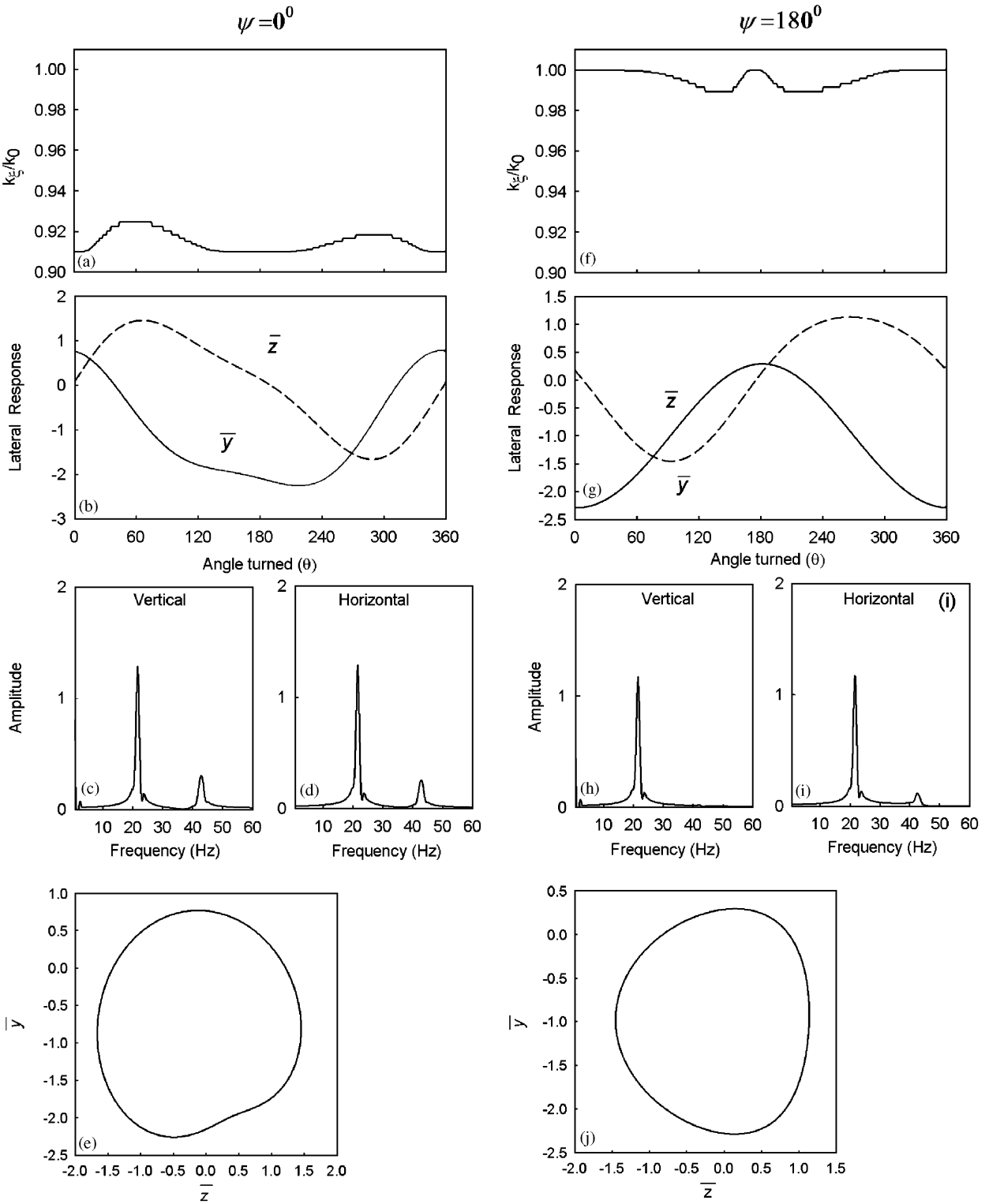

Fig. 7. Stiffness ratio variation, time domain response, frequency domain response and orbit plot of the cracked bowed rotor for large bow amplitude ($\bar{R}_0 = 10$, $\psi = 0^\circ$ and 180°).

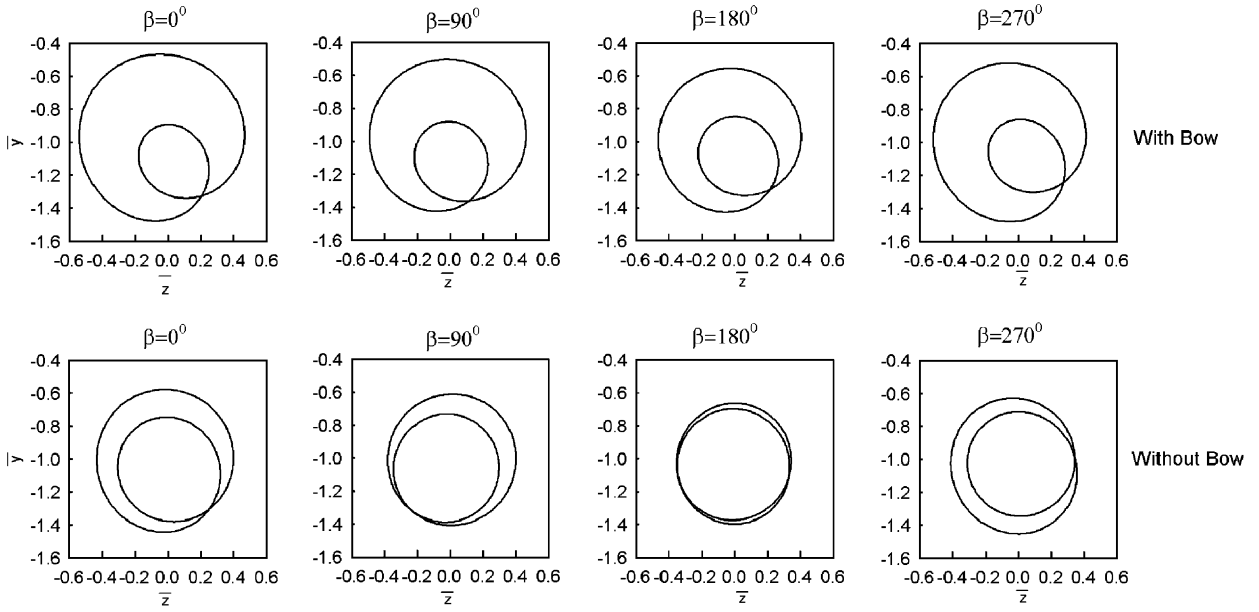

Fig. 8. Influence of unbalance phase relative to crack on the response of the cracked bowed rotor ($\psi = 0^{\circ}$).

loop orientation of the orbit plot. This has been highlighted as one of the important way in identifying the presence of crack [7]. However, Fig. 8 shows that in presence of bow, the absence of any changes in orbit plot with unbalance phase could give incorrect interpretation. The presence of bow masks changes in the orbit plot with unbalance phase and it may be mentioned that the influence of the bow is predominant over the influence of phase of unbalance.

Response of the cracked bowed rotor at $\frac{1}{3}$rd of the critical speed is now investigated for $\bar{a} = 0.3$ and $\beta = 0^{\circ}$. The simulation at this speed is done to ascertain the effect of bow, if any on the response of the cracked rotor. Since the response at $\frac{1}{3}$rd critical speed is important for the crack detection, it is important to investigate whether any significant changes occur in the response of the cracked rotor at this speed, if a bow exists for the cracked rotor. Fig. 9 shows the response for three cases, namely, cracked rotor response without bow, with bow at $\psi = 0^{\circ}$ and with bow at $\psi = 180^{\circ}$ $\left(\bar{R}_0 = 1\right)$. It may be observed from Figs. 9c and d that the third harmonic component is dominant in the response with the $3\times$ frequency component stronger in the horizontal direction than in the vertical direction and the orbit plot shows two distinct and large internal loops. When the bow is present in the direction of crack ($\psi = 0^{\circ}$), the frequency domain response shows increased $1\times$ component; an amplitude of 0.136 compared to 0.034 without bow in the vertical direction and an amplitude of 0.126 compared to 0.023 in horizontal direction (Figs. 9h and i). However, it may be noted that the amplitude of the $3\times$ frequency component has not changed compared to the one without bow (Figs. 9c,d). The amplitudes of $3\times$ frequency component in the vertical and horizontal directions (0.045 and 0.067, respectively) are same for without bow and with bow cases. However due to the increased difference between the $1\times$ and $3\times$ amplitudes, the orbit plot (for $\psi = 0^{\circ}$) shows very small inner loops and the orbit looks stretched along 45° (Fig. 9j). When the bow is in opposite phase to the crack direction, the amplitude of $1\times$ frequency component is considerably reduced compared to the case of $\psi = 0^{\circ}$ (Figs. 9m and n) and the orbit plot shows increased size of the inner loops (Fig. 9o). The presence of rotor bow distorts the shape of orbit that is observed with cracked rotor without bow.

The above investigations provide important information regarding the effect of bow. The results presented above can explain the difference in the orbit plot obtained with the cracked rotor experimentally and the one observed analytically. The authors have reported experimental investigations on transient response of two cracked rotors of different depths [35]. The orbit plots experimentally recorded for both the cracked rotors are shown in Fig. 10. It may be noted that for the first rotor with crack depth of $\bar{a} = 0.34$ (Fig. 10d), orbit plot at one-third critical speed is quite matching with the analytical results for the unbowed cracked rotor (Fig. 9e).

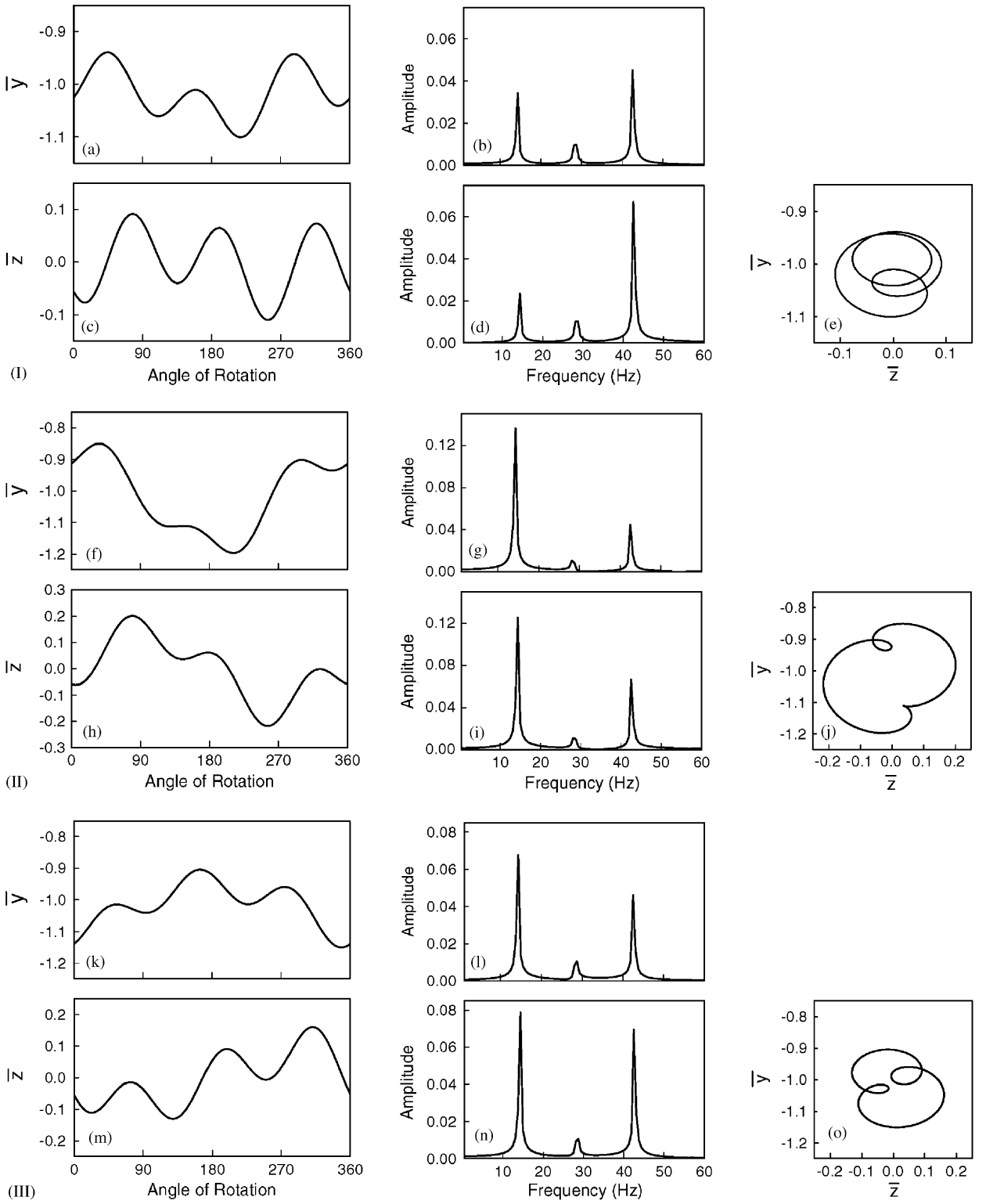

Fig. 9. Response of a cracked rotor with bow ($\bar{a} = 0.3$ $r_{unb} = 1/3$ and $\beta = 0^\circ$); cracked rotor: (I) without bow (II), with a bow at $\psi = 0^\circ$ (III) with a bow at $\psi = 180^\circ$; time domain response in: (a, f, k) vertical and (b, g, l) horizontal directions. Frequency domain response in: (c, h, m) vertical and (d, i, n) horizontal directions; (e, j, o) orbit plot.

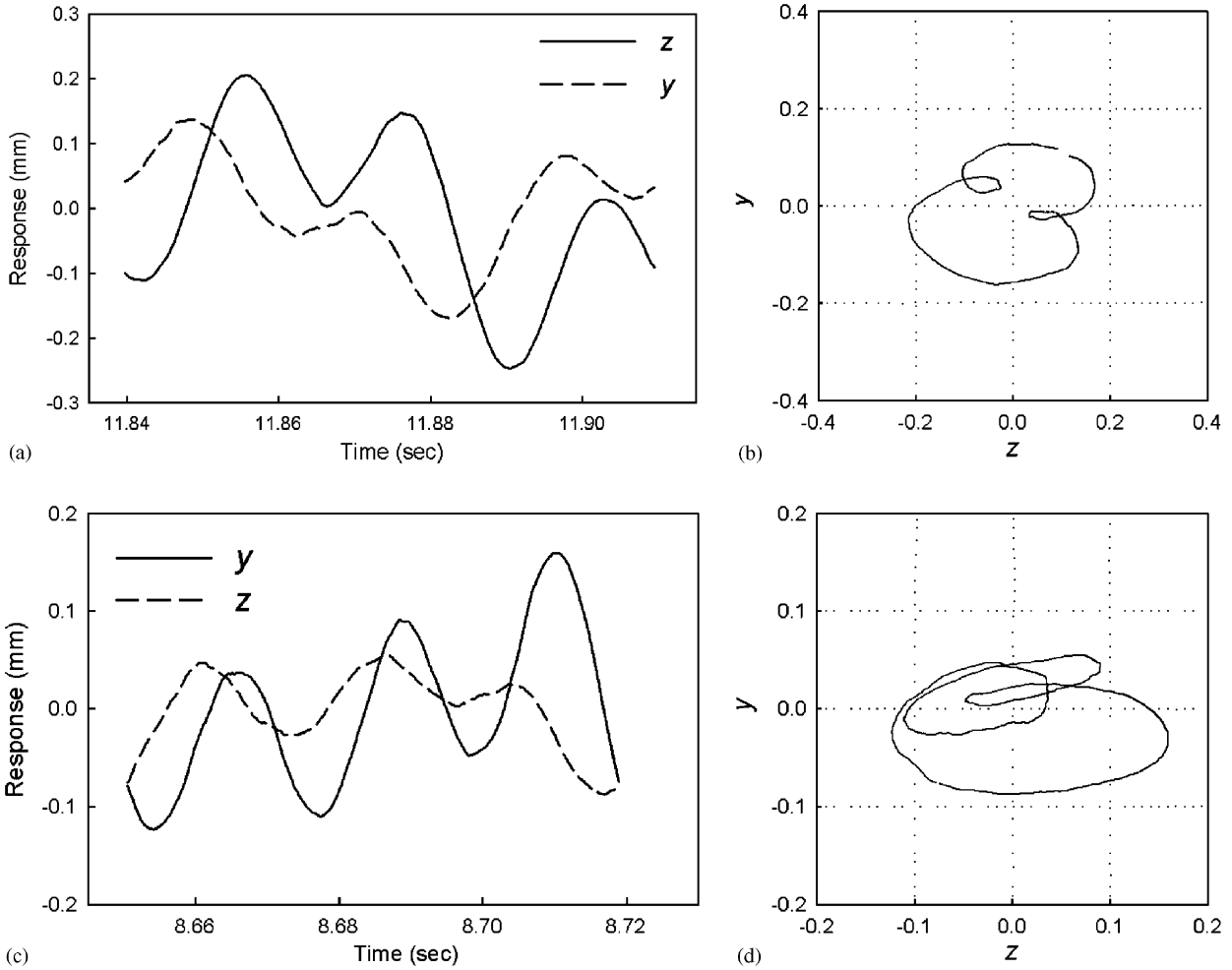

Fig. 10. Experimental response of a cracked rotor: (a) and (b) cracked rotor with $\bar{a} = 0.23$; (c) and (d) cracked rotor with $\bar{a} = 0.37$ [35].

However, for the second rotor with crack depth of $\bar{a} = 0.23$ (Fig. 10b), the orbit plot has the inner loops distorted and matching with the analytical results for the bowed cracked rotor (Fig. 9j). Thus the rotor could have some bow which influences the orbit plot. The results presented in this section, however, also show that the presence of higher harmonic components and the directional nature of these harmonic components are still valid despite the presence of the bow in the cracked rotor.

Thus the cracked rotor response at $\frac{1}{2}$ and $\frac{1}{3}$rd critical speed shows the influence of bow in the form of an increased $1\times$ amplitude and the changes in the orbit plot of the rotor. However, the higher harmonics do not show any changes in their amplitude in the presence of the additional forces due to bow. These harmonics, as is well known, depend on gravity. The influence of gravity is much stronger than the influence of bow. This is evident from the stiffness variation of the cracked bowed rotor. In Fig. 4a in absence of gravity, the bow has kept the crack open when it was in the direction of crack and kept it closed (Fig. 4e) when it was acting opposite to the direction of crack. However, in the presence of gravity, Figs. 5a,e and 6a,e do not show any significant influence on the stiffness variation when the phase of bow is varied.

4. Transient response of the cracked bowed rotor

An important bow indicator is the self-balancing speed, where the response of the rotor becomes zero. However for the uncracked rotor, this happens in the case of ψ close to 180° and the self-balancing speed is

observed at $\omega = \omega_0\sqrt{\bar{R}_0}$ i.e., at $\Omega = \sqrt{\bar{R}_0}$. For the cracked rotor, from the right-hand side of Eqs. (20), if gravity and ${\omega_{\xi\eta}}^2$ is neglected, this self-balancing speed is given by $\omega = \omega_\xi\sqrt{\bar{R}_0}$, i.e., $\Omega_{sb} = r_\xi\sqrt{\bar{R}_0}$. Thus due to the influence of gravity on the cracked rotor response, the self-balancing speed may not be observed for the cracked bowed rotor. In other words, the zero amplitude response at self-balancing speed may not be observed for a bowed cracked rotor.

To investigate the influence of the presence of crack on the self-balancing speed observed in the case of uncracked bowed rotor, the equations of motion of cracked bowed rotor presented in previous section are modified to include angular acceleration terms. The resulting equations are for the transient response of the accelerating cracked rotor with residual bow and are given below.

$$\begin{aligned} &m\ddot{\xi} + c\left(\dot{\xi} - \omega\eta\right) - 2\omega\dot{\eta}m - m\omega^2\xi + k_\xi(\xi - R_0\cos\psi) + k_{\xi\eta}(\eta - R_0\sin\psi)\\ &\quad = m\varepsilon\omega^2\cos\beta - mg\cos\omega t + m\varepsilon\ddot{\theta}\sin\beta,\\ &m\ddot{\eta} + c(\dot{\eta} + \omega\xi) + 2\omega\dot{\xi}m - m\omega^2\eta + k_{\eta\xi}(\xi - R_0\cos\psi) + k_\eta(\eta - R_0\sin\psi)\\ &\quad = m\varepsilon\omega^2\sin\beta + mg\sin\omega t - m\varepsilon\ddot{\theta}\cos\beta. \end{aligned} \tag{24}$$

Introducing the following dimensionless parameters:

$$\begin{gathered} \bar{\xi} = \xi/\delta_{st}, \quad \bar{\eta} = \eta/\delta_{st}, \quad \bar{R}_o = R_o/\delta_{st}, \quad \tau = \omega_0 t, \quad \Omega = \omega/\omega_0, \quad \lambda = \ddot{\theta}/\omega_0\\ r_\xi = \omega_\xi/\omega_0, \quad r_\eta = \omega_\eta/\omega_0, \quad r_{\xi\eta} = \omega_{\xi\eta}/\omega_0, \quad r_{\eta\xi} = \omega_{\eta\xi}/\omega_0 \end{gathered} \tag{25}$$

and $\omega_0 = \sqrt{k_0/m}$, where k_0 is the stiffness of uncracked rotor, Eqs. (24) can be non-dimensionalised as

$$\begin{aligned} &\ddot{\bar{\xi}} + 2\zeta(\dot{\bar{\xi}} - \bar{\eta}\Omega) - 2\dot{\bar{\eta}}\Omega - \left(r_0^2 - r_\xi^2\right)\bar{\xi} + r_{\xi\eta}^2\,\bar{\eta} = e\Omega^2\cos\beta - \cos\tau\\ &\quad + e\lambda\sin\beta + \bar{R}_o r_\xi^2\cos\psi + \bar{R}_o r_{\xi\eta}^2\sin\psi,\\ &\ddot{\bar{\eta}} + 2\zeta(\dot{\bar{\eta}} + \bar{\xi}\Omega) + 2\dot{\bar{\xi}}\Omega - \left(r_0^2 - r_\eta^2\right)\bar{\eta} + \bar{\xi}r_{\eta\xi}^2 = e\Omega^2\sin\beta + \sin\tau\\ &\quad - e\lambda\cos\beta + \bar{R}_o r_\eta^2\sin\psi + \bar{R}_o r_{\eta\xi}^2\cos\psi. \end{aligned} \tag{26}$$

Eqs. (26) are numerically integrated using Runge–Kutta method with $\bar{R}_0 = 0.5$, $\beta = 0^\circ$ $\psi = 180^\circ$ and $\lambda = 0.001$ ($75\,\mathrm{rad/s^2}$). To facilitate comparison with an uncracked rotor, initially a simulation is carried out for an uncracked rotor ($\bar{a} = 0$). The responses of the uncracked rotor (Fig. 11b) and cracked rotor (Fig. 11d) in presence of bow are compared in Fig. 11. Fig. 1b shows zero response at self-balancing speed at $\Omega_{sb} = 0.7$ ($\tau = 635$). When the response is estimated for a cracked rotor with $\bar{a} = 0.3$, the above-mentioned self-balancing speed is not quite clearly observed in the response (Fig. 11d). It should be noted that the so-called self-balancing speed could exist for cracked rotor only in absence of gravity and the non-zero response at Ω_{sb} is expected for the cracked bowed rotor. The term 'self-balancing' speed used in the context of cracked bowed rotor is just for the sake of comparison with uncracked bowed rotor. The self-balancing speed for the cracked bowed rotor can be observed in vertical rotors without any radial preload provided bow is opposite the crack.

The response of the cracked rotor with bow is compared with that of the cracked rotor without bow. The response of the cracked rotor without bow is shown in Fig. 11f. Near the 'self-balancing' speed (at $\tau = 635$), the response of the cracked rotor without bow is approximately $\bar{y} = 0.16$ as against $\bar{y} = 0.07$ for the cracked rotor with bow. Thus the presence of bow (out of phase with crack) in the cracked rotor reduces the amplitude of the response at the 'self-balancing' speed. In addition to the response, the stiffness ratio variation is also shown in the figure. Comparing the stiffness ratio variation for the cracked rotor with and without bow in Figs. 11c and e, respectively, the existence of bow tends to keep the crack closed for most of the period during transient passage as it is in opposite phase with the crack. However, near the 'self-balancing' speed, the stiffness ratio variation does not show any difference between the two cases of with bow and without bow. Thus the breathing, as expected, is strongly influenced by gravity in this region away from the critical speed. However, in the critical speed region ($\tau = 800 - 1000$) the bow influences the breathing behaviour of the crack.

The effect of gravity on the response of the cracked bowed rotor is significant. The response of the cracked bowed rotor is estimated neglecting the gravity. The response is shown in Fig. 11h. The response drops to zero at the self-balancing speed, which is clearly observed. The stiffness ratio variation in this case shows that the

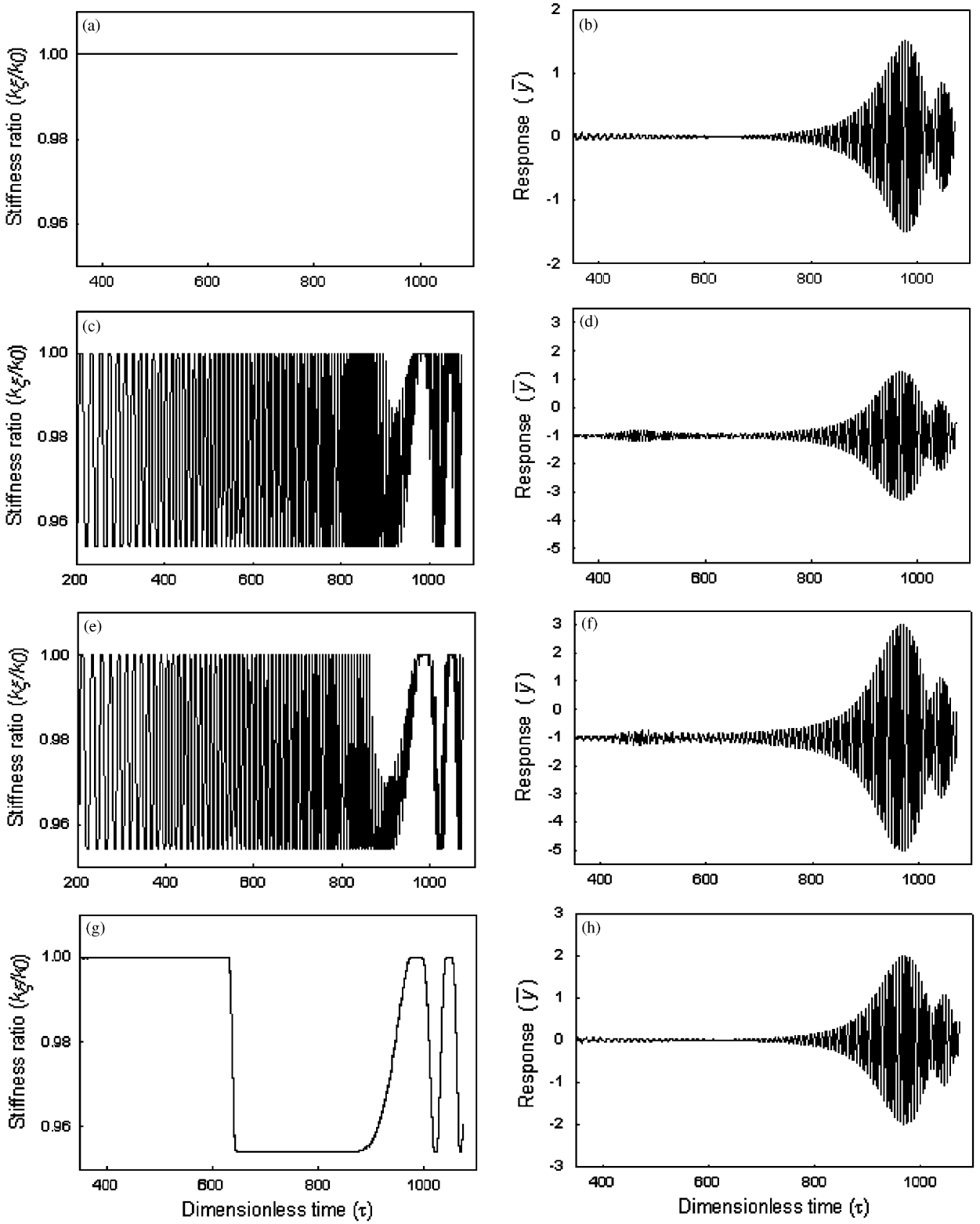

Fig. 11. Stiffness ratio variation and response of: (a,b) uncracked bowed rotor; (c,d) cracked bowed rotor; (e,f) cracked unbowed rotor; (g,h) cracked bowed rotor without gravity ($\bar{R}_0 = 0.5$, $\beta = 0^\circ$ $\psi = 180^\circ$).

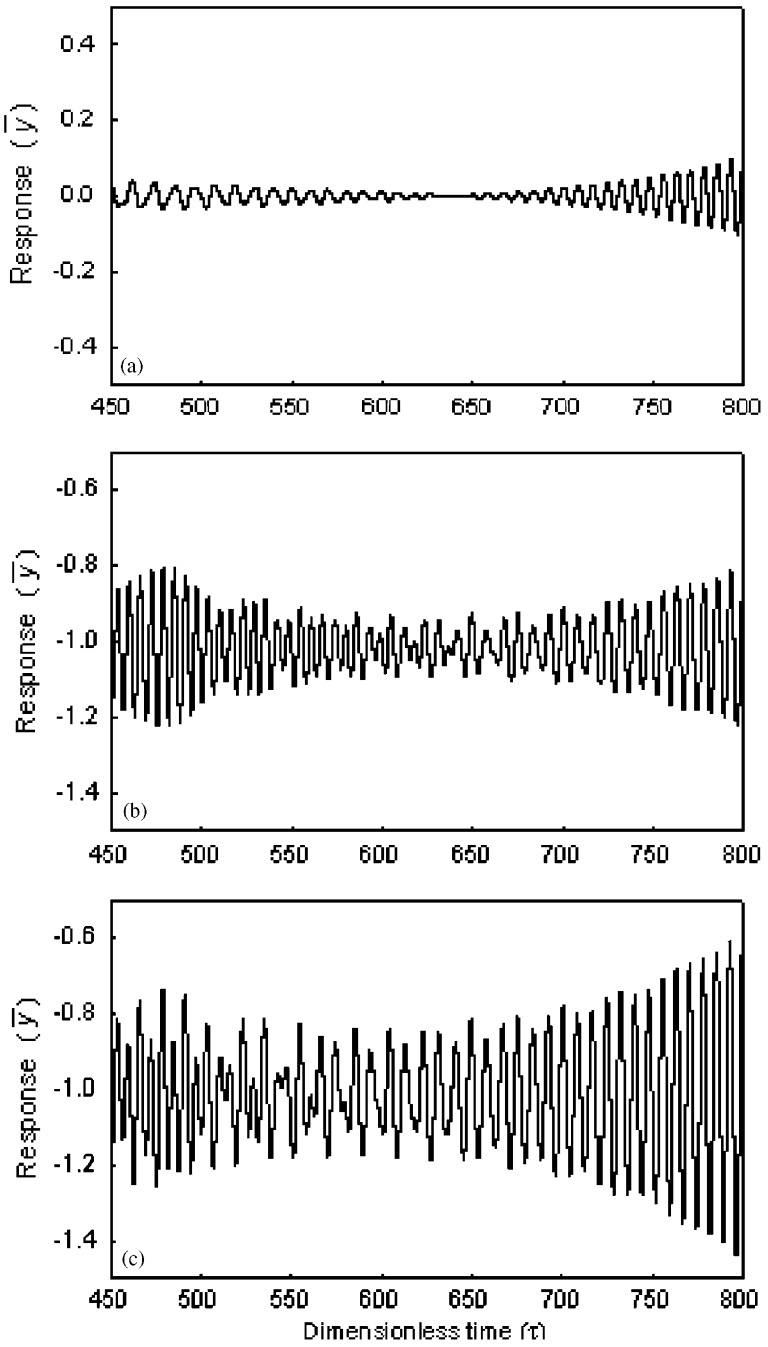

Fig. 12. Close-up view of the response near self-balancing speed; (a) uncracked bowed rotor; (b) cracked bowed rotor; (c) cracked rotor without bow.

crack remains closed under the influence of bow till the self-balancing speed and it suddenly opens at the self-balancing speed (at$\tau = 635$). The sudden phase change that is established in the case of uncracked bowed rotor for $\psi = 180^\circ$ [13], is observed here in case of the cracked rotor if the gravity is neglected in the analysis.

Fig. 12 shows the close-up view of the response near self-balancing speed. The drop in the response amplitude for the cracked rotor in presence of bow is noticed from Figs. 12b and c. Similarly the zero response

at the self-balancing speed for the uncracked rotor observed in Fig. 12a is not seen in Fig. 12b for the cracked bowed rotor.

Because of the gravity response, the 'self-balancing' speed for the cracked bowed rotor is not noticed and the response does not drop to zero at this speed as in case of the uncracked bowed rotor. Thus if the previous coast up signals are available for comparison, a drop in the amplitude level of the cracked rotor response in the future coast up signal can be related to the contribution of bow in the rotor. Alternatively, the disappearance of the zero response at the self-balancing speed from the coast-up signal of the uncracked bowed rotor may indicate the presence of crack. It may be mentioned that these observations are applicable only for the case of bow existing in opposite direction to that of the crack.

5. Conclusions

Equations of motion of a cracked rotor with bow are formulated. The effect of rotor bow on the breathing behaviour of the cracked rotor is investigated for various values of bow intensity. For normal values of bow, the gravity dominates the breathing behaviour of the cracked rotor. The amplitudes of higher harmonic components in the cracked rotor response and their directional nature remains unaltered due to rotor bow, however, expectedly the rotational frequency component changes in amplitude. The orbit plot at second harmonic resonant speed changes the orientation depending on the direction of rotor bow. Similarly, the rotor bow masks the sensitivity of cracked rotor response to the unbalance phase at this speed and exhibits more or less similar orbital response for different unbalance phase. This result is important from the viewpoint of crack diagnosis based on response at half critical speed.

The transient response of the cracked bowed rotor with and without gravity has been analysed. The self-balancing speed observed for uncracked bowed rotor is not observed for cracked bowed rotor if the gravity is considered in the analysis. If the cracked rotor is being monitored, the reduction in the amplitude of the response during coast-up at self-balancing speed could indicate the presence of bow in the cracked rotor. Similarly, if the bowed rotor is being monitored, the presence of non-zero response amplitude at the self-balancing speed could indicate the growing transverse crack in the rotor.

References

[1] J. Wauer, On the dynamics of cracked rotors—a literature survey, *Applied Mechanics Reviews* 43 (1990) 13–17.
[2] A.D. Dimarogonas, Vibration of cracked structures: a state of the art review, *Engineering Fracture Mechanics* 55 (1996) 831–857.
[3] R.A. Gasch, Survey of the dynamic behavior of a simple rotating shaft with a transverse crack, *Journal of Sound and Vibration* 160 (1993) 313–332.
[4] K. Gupta Rotor crack detection strategies—a review, *National Symposium on Rotor Dynamics (NSRD-2003)*, IIT, Guwahati, India, 15–17, December 2003.
[5] G. Sabnavis, R.G. Kirk, M. Kasarda, D. Quinn, Cracked shaft detection and diagnostics: a literature review, *The Shock and Vibration Digest* 36 (2004) 287–296.
[6] I. Imam, S.H. Azzaro, R.J. Bankert, J. Scheibel, Development of an on-line rotor crack detection and monitoring system, *Journal of Vibration, Acoustics, Stress and Reliability in Design* 111 (1989) 241–250.
[7] O.S. Jun, H.J. Eun, Y.Y. Earmme, C.W. Lee, Modeling and vibration analysis of a simple rotor with a breathing crack, *Journal of Sound and Vibration* 155 (1992) 273–290.
[8] K.R. Collins, R.H. Plaut, J. Wauer, Detection of cracks in rotating Timoshenko shafts using axial impulses, *Journal of Vibration and Acoustics* 113 (1991) 74–78.
[9] C.A. Papadopoulos, A.D. Dimarogonas, Coupled vibration of cracked shafts, *Journal of Vibration and Acoustics* 114 (1992) 461–467.
[10] A.K. Darpe, K. Gupta, A. Chawla, Coupled Bending, Longitudinal And Torsional Vibrations Of A Cracked Rotor, *Journal of Sound and Vibration* 269 (2004) 33–60.
[11] S. Edwards, A.W. Lees, M.I. Friswell, Fault diagnosis of rotating machinery, *Shock and Vibration Digest* 30 (1998) 4–13.
[12] R. Platz, R. Markert, 2001, Fault models for online identification of malfunction in rotor systems, Transactions of the fourth International Conference, Acoustical and Vibratory Surveillance, Methods and Diagnostic Techniques, University of Compiegne, France, 16–18 October, 2001, pp. 435–446.
[13] J.C. Nicholas, E.J. Gunter, P.E. Allaire, Effect of residual shaft bow on unbalance response and balancing of a single mass flexible rotor. Part 1: unbalance response, *Journal of Engineering for Power* (1976) 171–181.
[14] D.J. Salamone, Synchronous Unbalance Response of a Multimass Flexible Rotor Considering Shaft Warp and Disk Skew, MS Thesis, University of Virginia, May 1977.

[15] R.D. Flack, J.H. Rooke, A theoretical-experimental comparison of the synchronous response of a bowed rotor in five different sets of fluid film bearings, *Journal of Sound and Vibration* 73 (1980) 505–517.
[16] R.D. Flack, J.H. Rooke, J.R. Bielk, E.J. Gunter, Comparison of the unbalance responses of Jeffcott rotors with shaft bow and shaft runout, *Journal of Mechanical Design. Transactions of ASME* 104 (1982) 318–328.
[17] P. Gnielka, Modal balancing of flexible rotors without test runs: an experimental investigation, *Journal of Sound and Vibration* 90 (1983) 157–172.
[18] A.G. Parkinson, Balancing of rotating machinery. *Proceedings of the Institution of Mechanical Engineers Part C—Mechanical Engineering Science*, Vol. 205, 1991, pp. 53–66.
[19] W.L. Meacham, P.B. Talbert, H.D. Nelson, N.K. Cooperrider, Complex modal balancing of flexible rotors including residual bow, *Journal of Propulsion and Power* 4 (1988) 245–251.
[20] H.D. Nelson, Steady synchronous response and balancing of rotor systems with residual shaft bow, *International Journal of Rotating Machinery* 8 (2002) 431–438.
[21] J.S. Rao, A note on Jeffcott warped rotor, *Mechanism and Machine Theory* 36 (2001) 563–575.
[22] F.F. Ehrich, *Handbook of Rotordynamics*, McGraw Hill, New York, 1992.
[23] P. Goldman, A. Muszynska, Rotor-to-stator, Rub-related, Thermal/Mechanical Effects in Rotating Machinery, *Chaos, Solitons and Fractals* 5 (1995) 1579–1601.
[24] P. Goldman, A. Muszynska, D.E. Bently, Thermal Bending of rotor due to rotor-to-stator bow, *International Journal of Rotating Machinery* 6 (2000) 91–100.
[25] S. Edwards, A.W. Lees, M.I. Friswell, Experimental identification of excitation and support parameters of a flexible rotor-bearings-foundation system from a single run-down, *Journal of Sound and Vibration* 232 (2000) 963–992.
[26] N. Bachschmid, P. Pennacchi, Model based malfunction identification from bearing measurements, Institution of Mechanical Engineers Conference Transactions, *Seventh International Conference on Vibration in Rotating Machinery*, Nottingham, UK, 12–14 September, 2000. pp. 571–580.
[27] R. Platz, R. Markert, M. Seidler, Validation of online diagnostics of malfunctions in rotor systems, Institution of Mechanical Engineers Conference Transactions, *Seventh International Conference on Vibration in Rotating Machinery*, Nottingham, UK, 12–14 September, 2000. pp. 581–590.
[28] N. Bachschmid, P. Pennacchi, A. Vania, Identification of multiple faults in rotor systems, *Journal of Sound and Vibration* 254 (2002) 327–366.
[29] P. Pennacchi, A. Vania, Accuracy in the identification of a generator thermal bow, *Journal of Sound and Vibration* 274 (2004) 273–295.
[30] A.K. Darpe, K. Gupta, A. Chawla, Dynamics of a two-cracked rotor, *Journal of Sound and Vibration* 259 (2003) 649–675.
[31] F. Wan, Q. Xu, S. Li, Vibration analysis of cracked rotor sliding bearing system with rotor-stator rubbing by harmonic wavelet transform, *Journal of Sound and Vibration* 271 (2004) 507–518.
[32] I.W. Mayes, G.R. Davis, The vibrational behavior of a rotating shaft system containing a transverse crack, *Vibrations in Rotating Machineries—Proceedings of the International Conference*, Institution of Mechanical Engineers, 1976, pp. 53–64.
[33] A.K. Darpe, A. Chawla, K. Gupta, Analysis of the response of a cracked Jeffcott rotor to axial excitation, *Journal of Sound and Vibration* 249 (2002) 429–445.
[34] H. Tada, P.C. Paris, G.R. Irwin, *The Stress Analysis of Crack Handbook*, Del Research Corporation, Hellertown, PA, 1973.
[35] A.K. Darpe, K. Gupta, A. Chawla, Transient response and breathing behaviour of a cracked Jeffcott rotor, *Journal of Sound and Vibration* 272 (2004) 207–243.